A Novel Design of a SIW-Fed Antenna Array Using an Accelerated Full-Wave Methodology

Alfonso Gómez García, Jesús Rubio, Jose Luis Masa-Campos, Juan Córcoles *Senior Member, IEEE*, Yolanda Campos Roca, and Rafael Gómez Alcalá *Member, IEEE*,

***Abstract*—Arrays fed by substrate integrated waveguides (SIWs) are a current topic of interest. However, most designers have to rely on general purpose commercial software, usually inefficient for multiple full-wave simulations in a design process. This work proposes a new fast full-wave strategy, with very low iteration times, based on the simultaneous use of addition theorems for spherical and cylindrical modes. After a domain decomposition of the array into fixed or modifiable (to be optimized) sections, each section is analyzed using a finite-element/modal analysis to obtain its general scattering matrix. Fixed sections are only once coupled at the beginning, while each optimization iteration is calculated with full-wave precision by adding the interactions with the modifiable sections. A complete design process of a novel 16-slot progressive-wave SIW-fed array is performed to validate the strategy usefulness. 112800 iterations, with 47 optimization variables, are calculated in under 4 hours (speed-up factor of over 2000 compared to general purpose commercial software). The designed device is manufactured and experimentally characterized, measuring a 1.05 GHz $|S_{11}|$ bandwidth under -10 dB, and a maximum gain of 15.6 dBi at θ=-11° in the array plane.**

***Index Terms*—Addition theorems, cylindrical modes, spherical modes, optimization process, antenna array, substrate integrated waveguide (SIW).**

I. Introduction

SUBSTRATE integrated waveguide (SIW) tecnology has been a topic of interest for many researchers in the last few years, due to its capability to combine the high-power handling properties of traditional rectangular waveguides with the fabrication techniques used in printed circuit boards (PCBs). SIW devices are based on the use of metallized via holes to connect the two metal layers of a dielectric substrate, with rules on the size and separation of said via holes [1], [2].

Slot antenna arrays placed on the top-plate of a SIW can be found quite early in the literature [3], [4], [5], [6], [7], [8], [9], [10], [11], [12]. More complex structures that modify the basic slot radiating element, such as the use of dielectric resonators placed on top of the slot [13], [14], [15], have been reported. Resonant patch antennas, where the SIW is used as a resonant cavity, are also common [16], [17], [18], [19]. Even SIW-based leaky-wave antennas [20], [21], [22] or horn antennas [23], [24] are present in the literature.

Nevertheless, most of these devices have been designed using commercial full-wave software, which is not known for its fast iteration times in a design process. Some works use a circuital approach [8], [14], [10], [11], [12], [21], aggressive space mapping [25] or Elliot's formulas [6], [11], but yet a full-wave simulation of the device is usually needed to precisely tune and validate the design.

To the best of the authors' knowledge, only another fast hybrid full-wave methodology to analyze SIW-fed antenna arrays had been proposed in previous works. In [26], [27] the Method of Moments (MoM) is hybridized with mode-matching (MM) to obtain fast iteration cycles with full-wave precision when working with antenna slots fed by SIW. This method exhibits very low iteration times, but it is limited by its application to just antenna slots fed by SIW.

Recently, we have introduced a hybrid full-wave methodology based on a finite-element/modal analysis (FE/MA) with fast frequency sweep and modal expansion in cylindrical modes for the fast analysis of SIW circuits in [28]. Later, it was extended to the analysis of antenna arrays placed on the top plate of a SIW by the simultaneous use of the addition theorems for spherical and cylindrical modes, in [29]. This methodology is based on the division of the SIW device into different sections bounded by cylindrical ports, and by hemispherical ports if a radiating element is contained in the considered section. The general scattering matrix (GSM) of each section is obtained using the FE/MA solver with fast frequency sweep, but any other methods able to obtain GSMs are suitable. The use of FE/MA allows the analysis of arrays of different types of elements such as arbitrarily shaped apertures, patches, or dielectric resonator antennas (DRAs) at the expense of a lesser memory saving (compared to other works in the literature). Once the GSMs of all the different sections have been obtained, cylindrical and spherical addition theorems are used simultaneously to obtain the behavior of the analyzed device.

In this work, we propose a different strategy using a new formulation of the problem based on the sequential coupling of fixed and modifiable sections in each iteration of an optimization process. This new strategy allows us to accelerate the aforementioned methodology. In the new formulation, a

This work was supported by MINECO/AEI/FEDER, European Union, Spain, under project TEC2017-83352-C2-2-P; by FEDER program (European Union) and Junta de Extremadura under projects GR18055 and GR21072; by the Spanish Ministry of Science, Innovation and Universities under the State Subprogram for Research Infrastructures and Scientific-Technical Equipment via the RF Prototyping and Measurement Lab with reference EQC2019-005583-P; by the Spanish Government under grant PID2020-116968RB-C32 (DEWICOM) funded by MCIN/AEI/ 10.13039/501100011033 (Agencia Estatal de Investigación); and by the Spanish Ministry of Education, Culture and Sport (MECD) via a PhD grant to A. Gómez García (FPU17/00825).

A. Gómez García, J. Rubio., Y. Campos Roca and R. Gómez Alcalá are with Escuela Politécnica, Universidad de Extremadura, 10003 Cáceres, Spain. (e-mail: alfonsogg@unex.es;jesusrubio@unex.es).

J. L. Masa Campos and J. Córcoles are with Escuela Politécnica Superior, Universidad Autónoma de Madrid, 28049 Madrid, Spain. (e-mail: joseluis.masa@uam.es).

group of fixed sections is established at the beginning of an optimization process, and the interactions between them are calculated only once. The elements modified, by using either a different geometry or position on the design, are then coupled between them and to the other sections of the device in each iteration. With this new strategy, lower iteration times can be obtained in contrast to performing the simultaneous coupling of all the sections of the device. It should be noted that the proposed methodology will provide better iteration times the greater the total number of modes from fixed sections is, compared to those from modifiable ones. More specifically, since the metallized via holes that form the SIW walls are neither geometrically changed nor moved, and they are much greater in number than the usually optimized radiating elements, much lower iteration times can be obtained.

In order to test the validity and utility of the new proposed strategy, a full design process of a progressive wave 16 transversal slot SIW antenna linear array is carried out. Apart from the known advantages of SIW technology, it also allows for near-broadside radiation, greatly in contrast with traditional hollow rectangular waveguides [30], [**?**]. The use of the proposed method allows to consider in a single step the complete interactions between the slots. As a result, a novel design where the physical dimensions of the slots do not follow a monotonic tendency to increase the adaptation, and no additional matching elements are needed, has been obtained. The optimization of the distance between elements, as also the width and length of each individual slot, has resulted in a design that contrasts with the traditional literature [3], [4], [5], [6], [7]. The criteria, algorithm and limits of the different variables used in the optimization process are also discussed. The computational time of each iteration of the optimization process is also compared to those obtained if our previous work was to be used instead. Additional simulations with the CST Studio Suite 2020 [31] are also performed to validate the formulation.

The final design, with a size of $9.17\lambda_0$ at $17\,\mathrm{GHz}$, is manufactured and measured, obtaining a $15.6\,\mathrm{dBi}$ measured gain near-broadside, with over a $1.0\,\mathrm{GHz}$ measured bandwidth under $-10\,\mathrm{dB}$ in terms of $|S_{11}|$. The manufactured design also has a 98.5% measured impedance mismatch factor (defined as the ratio of the power accepted by the antenna to the power incident at the antenna terminals), resulting in a 64.4% estimated total efficiency. These results, hard to be simultaneously obtained in the current state of the art [21], [32], [20], [33], [34], are obtained due to the capability of the methodology to consider all the interactions within the array in an optimization process with low iteration times.

II. Theory

The new proposed strategy follows the block diagram shown in Fig. 1, where a zero step is also included. This zero step refers to the analysis and determination of the GSMs that characterize each section into which the SIW array is decomposed, and the assignation of fixed and modifiable sections. Feeding sections, as also the metallized via holes,

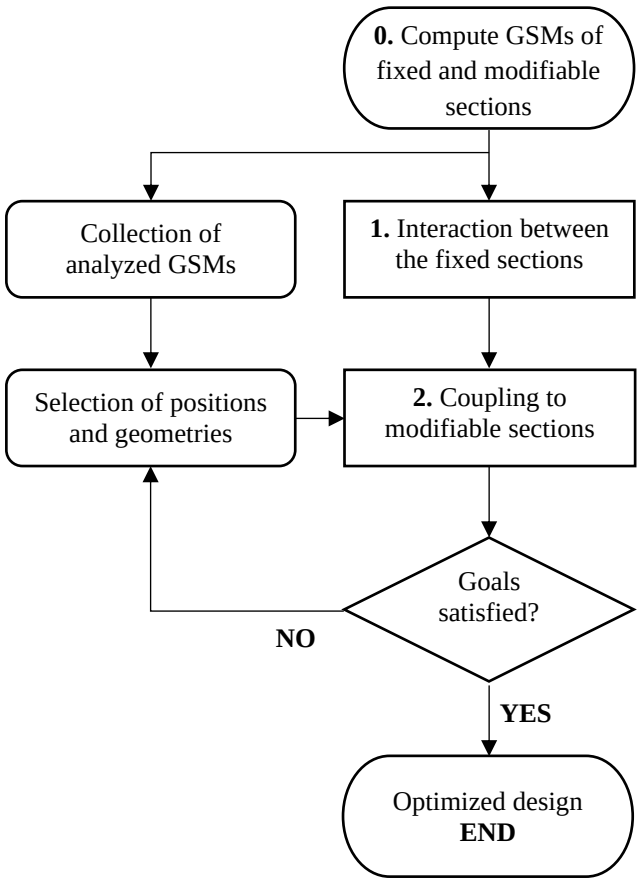

Figure 1. General block diagram of the new proposed strategy, with optimization loop.

can usually be considered fixed. Each possible geometry of the modifiable sections is also computed in this step, resulting in a discrete collection of analyzed geometries that can be easily and quickly loaded in each iteration of the optimization process. In this way, there is no need to compute any new GSM of any modifiable sections, since they can be just readily loaded from the collection computed in this step.

In general terms, three different section types can be defined in a usual single-layer SIW array: feeders, radiating elements, and scatterers (i.e., the metallized via holes). A feeder is defined as any section i that relates feeding modes, i.e. from a rectangular waveguide or a coaxial line, with cylindrical modes. Its GSM is structured as

$$\begin{bmatrix} \boldsymbol{\Gamma}^{(i)} & \mathbf{R}_c^{(i)} \\ \mathbf{T}_c^{(i)} & \mathbf{S}_c^{(i)} \end{bmatrix} \begin{bmatrix} \mathbf{v}^{(i)} \\ \mathbf{a}_c^{(i)} \end{bmatrix} = \begin{bmatrix} \mathbf{w}^{(i)} \\ \mathbf{b}_c^{(i)} \end{bmatrix}, \tag{1}$$

where $\mathbf{v}^{(i)}$ and $\mathbf{w}^{(i)}$ are column vectors of the complex amplitudes of the incident and reflected feeding modes, respectively, on the feeding port of a section i. The complex amplitudes of the standing and scattered cylindrical modes on the cylindrical port of section i are presented, respectively, in the column vectors $\mathbf{a}_c^{(i)}$ and $\mathbf{b}_c^{(i)}$. $\boldsymbol{\Gamma}^{(i)}$ is the reflection matrix, whose elements are the reflection and coupling parameters of the feeding modes. $\mathbf{T}_c^{(i)}$ is the transmission matrix, whose elements are

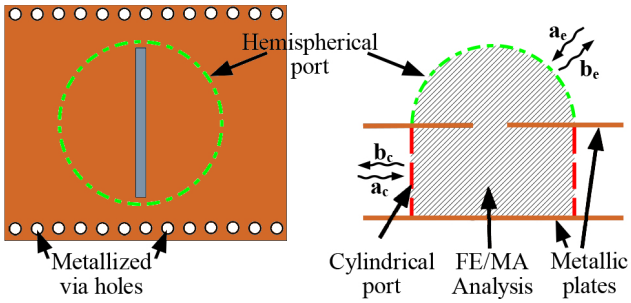

Figure 2. Top (left) and side (right) view of a slot placed on a SIW top plate.

the transmission coefficients between incoming feeding modes and outgoing cylindrical modes. On the other hand, $\mathbf{R}_c^{(i)}$ is the corresponding reception matrix between outgoing feeding and incoming cylindrical modes. Lastly, $\mathbf{S}_c^{(i)}$ is the scattering matrix of the cylindrical modes considered on the cylindrical port of section i. The use of standing cylindrical modes allows for a more compact formulation based on the source scattering matrix as defined by Yaghjian [36]. Nevertheless, it can be easily related to the classical scattering matrix in terms of incoming and scattering cylindrical modes [38].

The radiating elements are any section i that relates spherical modes with cylindrical modes, as it can be seen in Fig. 2. Their GSM can be summarized as

$$\begin{bmatrix} \mathbf{S}_e^{(i)} & \mathbf{C}_{ec}^{(i)} \\ \mathbf{C}_{ce}^{(i)} & \mathbf{S}_c^{(i)} \end{bmatrix} \begin{bmatrix} \mathbf{a}_e^{(i)} \\ \mathbf{a}_c^{(i)} \end{bmatrix} = \begin{bmatrix} \mathbf{b}_e^{(i)} \\ \mathbf{b}_c^{(i)} \end{bmatrix}, \tag{2}$$

where $\mathbf{a}_e^{(i)}$ and $\mathbf{b}_e^{(i)}$ correspond to the standing and scattered spherical modes on the hemispherical port, $\mathbf{S}_e^{(i)}$ takes account of the relation between standing and scattered spherical modes [35], [36], and $\mathbf{C}_{ec}^{(i)}$ and $\mathbf{C}_{ce}^{(i)}$ account for the coupling between spherical and cylindrical modes. This definition of radiating elements implies that this kind of section does not directly relate feeding modes to spherical modes.

The final type of section, the scatterers, can be defined as any section i that is only able to relate the complex amplitudes of the cylindrical modes present in its cylindrical port. Therefore, they have a very simple GSM, structured as

$$\left[\mathbf{S}_c^{(i)}\right] \left[\mathbf{a}_c^{(i)}\right] = \left[\mathbf{b}_c^{(i)}\right]. \tag{3}$$

There are analytical methods to obtain the GSM of the SIW metallized via holes, or from dielectric posts [37]. To obtain the GSM of the rest of the elements, we use the FE/MA solver proposed in [38].

From these GSMs, we define the following matrices that will be used in the rest of the methodology as a collection of diagonal block matrices, composed from the GSMs of all the sections considered in the analyzed device, as

$$\begin{gathered} \mathbf{\Gamma} = diag\left(\mathbf{\Gamma}^{(i)}\right); \mathbf{T}_c = diag\left(\mathbf{T}_c^{(i)}\right); \mathbf{R}_c = diag\left(\mathbf{R}_c^{(i)}\right); \\ \mathbf{C}_{ce} = diag\left(\mathbf{C}_{ce}^{(i)}\right); \mathbf{C}_{ec} = diag\left(\mathbf{C}_{ec}^{(i)}\right); \\ \mathbf{S}_c = diag\left(\mathbf{S}_c^{(i)}\right); \mathbf{S}_e = diag\left(\mathbf{S}_e^{(i)}\right). \end{gathered} \tag{4}$$

In a similar way, the complex amplitudes of the considered modes can be grouped in column vectors as

$$\mathbf{v} = \begin{pmatrix} \mathbf{v}^{(1)} \\ \vdots \\ \mathbf{v}^{(i)} \\ \vdots \\ \mathbf{v}^{(N)} \end{pmatrix}; \mathbf{w} = \begin{pmatrix} \mathbf{w}^{(1)} \\ \vdots \\ \mathbf{w}^{(i)} \\ \vdots \\ \mathbf{w}^{(N)} \end{pmatrix}; \mathbf{b}_x = \begin{pmatrix} \mathbf{b}_x^{(1)} \\ \vdots \\ \mathbf{b}_x^{(i)} \\ \vdots \\ \mathbf{b}_x^{(N)} \end{pmatrix}; \tag{5}$$

where N is the total number of considered sections, and x can be either c or e to denote scattered cylindrical ($\mathbf{b}_c$) or spherical ($\mathbf{b}_e$) modes, respectively. Additionally, $\mathbf{a}_c$ and $\mathbf{a}_e$ are defined in a similar manner.

Finally, as explained in [28], the interactions between the different cylindrical ports are taken into account by means of the general translational matrix for cylindrical modes, $\mathbf{G}_c^{(i,j)}$. This matrix relates the scattered cylindrical modes from the cylindrical port of section j to the incident cylindrical modes of section i. An analogous definition can be extracted for spherical modes, where $\mathbf{G}_e^{(i,j)}$ allows the consideration of arbitrary rotation and translation in a 3D space [36]. The generalized translation matrix created from these terms can be expressed as

$$\mathbf{G}_x = \begin{pmatrix} \mathbf{0} & \mathbf{G}_x^{(1,2)} & \cdots & \mathbf{G}_x^{(1,N_x)} \\ \mathbf{G}_x^{(2,1)} & \mathbf{0} & \ddots & \vdots \\ \vdots & \ddots & \ddots & \vdots \\ \vdots & \ddots & \mathbf{0} & \mathbf{G}_x^{(N_x-1,N_x)} \\ \mathbf{G}_x^{(N_x,1)} & \ddots & \mathbf{G}_x^{(N_x,N_x-1)} & \mathbf{0} \end{pmatrix}, \tag{6}$$

where, once again, x can be c or e to denote either cylindrical modes or spherical modes respectively, with N_c being the number of considered sections with cylindrical ports and N_e the number of considered sections with spherical, or in this case, hemispherical ports.

It is also in this step where the differentiation between fixed and modifiable sections is made. Contrary to [29], where all sections were coupled simultaneously, in this work we adopt a different strategy. This consists of first coupling the sections that will not change in the optimization process neither in shape nor in position, to later couple the modifiable sections with each other and with the fixed sections (see Fig. 1). As it was proven in [39], in the context of coupling of antennas in terms of equivalent dipoles, the result of this strategy is the same as the one obtained if we couple all the sections simultaneously. However, in an optimization process, the fixed sections only need to be coupled once at the beginning (step 1 in Fig. 1). This will save computational time if their number is large in comparison with the modifiable sections, as we will show later. Therefore, $\mathbf{G}_c$ can be divided into four sub-blocks to account for the coupling between the cylindrical ports of fixed and modifiable sections as

$$\mathbf{G}_c = \begin{pmatrix} \mathbf{G}_c^{mm} & \mathbf{G}_c^{mf} \\ \mathbf{G}_c^{fm} & \mathbf{G}_c^{ff} \end{pmatrix}, \tag{7}$$

where $\mathbf{G}_c^{ff}$ represents the application of the general translational theorems for cylindrical modes for only the fixed sections, $\mathbf{G}_c^{mm}$ is its counterpart for the modifiable sections. $\mathbf{G}_c^{fm}$ and $\mathbf{G}_c^{mf}$ are applied between fixed and modifiable sections, or modifiable and fixed, respectively.

The defined group column vectors in (5), as well as the diagonal block matrices constructed from the GSMs of the different sections in (4), will have superscripts to indicate if they refer to fixed or modifiable sections. In this way, $\mathbf{S}_c^f$ is the diagonal block matrix constructed from the cylindrical scatter sub-matrix of only the fixed sections. On the other hand, $\mathbf{S}_c^m$ is the corresponding matrix when considering only the modifiable sections.

A. Interaction between the fixed sections

In this first step, the interaction between the cylindrical ports of the considered fixed sections are taken into account, since no fixed spherical ports are considered. Most frequently, antennas use a feeding network that is designed and optimized independently from the radiating elements, and can be considered fixed, or non-modifiable, to the rest of the design. Other parameters are also usually fixed in the design, such as the maximum dimensions of the antenna, the distance between the SIW walls, or the number of radiating elements. Henceforth, the formulation will consider the feeding elements, whose GSM was described in (1), as fixed sections. Many metallized via holes will also be considered to be fixed, i.e. those composing the SIW walls, and will also be accounted for in this step.

The analysis between cylindrical ports has been previously resolved in [28], obtaining as a result the s-parameters of the feeding modes. Nevertheless, the assumption made in [29], that no field is coming from outside the considered group of cylinders, is not true any more. In the present work, the modifiable sections have a non-zero contribution. Therefore, the equations (6) and (7) from [29], when considering that the modifiable sections introduce outside field to the interaction between the fixed cylinder ports, result in

$$\mathbf{\Gamma}^f\mathbf{v} + \mathbf{R}_c^f\mathbf{G}_c^{ff}\mathbf{b}_c^f + \mathbf{R}_c^f\mathbf{a}_o = \mathbf{w}, \tag{8}$$

$$\mathbf{T}_c^f\mathbf{v} + \mathbf{S}_c^f\mathbf{G}_c^{ff}\mathbf{b}_c^f + \mathbf{S}_c^f\mathbf{a}_o = \mathbf{b}_c^f, \tag{9}$$

where $\mathbf{a}_o$ is the complex amplitude of the standing cylindrical modes on the fixed cylindrical ports due to the modifiable sections.

Hence, solving (9)

$$\left(\mathbf{I} - \mathbf{S}_c^f\mathbf{G}_c^{ff}\right)^{-1}\mathbf{T}_c^f\mathbf{v} + \left(\mathbf{I} - \mathbf{S}_c^f\mathbf{G}_c^{ff}\right)^{-1}\mathbf{S}_c^f\mathbf{a}_o = \mathbf{b}_c^f, \tag{10}$$

and inserting the result in (8) leads to

$$\begin{aligned}\left(\mathbf{\Gamma}^f + \mathbf{R}_c^f\mathbf{G}_c^{ff}\left(\mathbf{I} - \mathbf{S}_c^f\mathbf{G}_c^{ff}\right)^{-1}\mathbf{T}_c^f\right)\mathbf{v} + \left(\mathbf{R}_c^f + \right.\\ \left.\mathbf{R}_c^f\mathbf{G}_c^{ff}\left(\mathbf{I} - \mathbf{S}_c^f\mathbf{G}_c^{ff}\right)^{-1}\mathbf{S}_c^f\right)\mathbf{a}_o = \mathbf{w}.\end{aligned} \tag{11}$$

From (10) and (11), it is possible to extract the GSM considering only the cylindrical interactions between the fixed sections as follows

$$\mathbf{\Gamma}^{(c)f} = \mathbf{\Gamma}^f + \mathbf{R}_c^f\mathbf{G}_c^{ff}\left(\mathbf{I} - \mathbf{S}_c^f\mathbf{G}_c^{ff}\right)^{-1}\mathbf{T}_c^f \tag{12}$$

$$\mathbf{R}_c^{(c)f} = \mathbf{R}_c^f + \mathbf{R}_c^f\mathbf{G}_c^{ff}\left(\mathbf{I} - \mathbf{S}_c^f\mathbf{G}_c^f\right)^{-1}\mathbf{S}_c^f \tag{13}$$

$$\mathbf{T}_c^{(c)f} = \left(\mathbf{I} - \mathbf{S}_c^f\mathbf{G}_c^{ff}\right)^{-1}\mathbf{T}_c^f \tag{14}$$

$$\mathbf{S}_c^{(c)f} = \left(\mathbf{I} - \mathbf{S}_c^f\mathbf{G}_c^{ff}\right)^{-1}\mathbf{S}_c^f \tag{15}$$

where the superscript $(c)f$ indicates that these matrices are obtained from coupling the fixed cylindrical ports.

B. Coupling to modifiable sections

The second step of the proposed strategy is also the iterated step in an optimization process. In this step, the previously fixed matrices are used in conjunction with a unique set of defined positions and geometries of the modifiable sections. These positions and geometries can be different each time this step is performed, and they can be decided by the designer (i.e., when fine tuning a design) or an optimization algorithm.

This step results in the complete analysis of the device, obtaining both the final s-parameters of the feeding modes and the radiation pattern of the array. Since the followed procedure is similar to the one described in [29], a simplified version of the equation to obtain the S-Parameters is used as foundation. In this case, the waveguide feeding is performed solely through direct coupling to the cylindrical modes, represented by matrices $\mathbf{R}_c$ and $\mathbf{T}_c$. Therefore, the equation is reduced to

$$\begin{aligned}\Big[\mathbf{\Gamma}^{(g)} + \mathbf{R}_c^{(g)}\mathbf{G}_c^{(g)}\mathbf{P}\mathbf{T}_c^{(g)} + \\ + \mathbf{R}_c^{(g)}\mathbf{G}_c^{(g)}\mathbf{P}\mathbf{C}_{ce}^{(g)}\mathbf{G}_e\mathbf{M}^{-1}\mathbf{Q}\Big]\mathbf{v} = \mathbf{w},\end{aligned} \tag{16}$$

with

$$\mathbf{P} = \left(\mathbf{I} - \mathbf{S}_c^{(g)}\mathbf{G}_c^{(g)}\right)^{-1}, \tag{17}$$

$$\mathbf{M} = \mathbf{I} - \mathbf{S}_e\mathbf{G}_e - \mathbf{C}_{ec}^{(g)}\mathbf{G}_c^{(g)}\mathbf{P}\mathbf{C}_{ce}^{(g)}\mathbf{G}_e, \tag{18}$$

$$\mathbf{Q} = \mathbf{C}_{ec}^{(g)}\mathbf{G}_c^{(g)}\mathbf{P}\mathbf{T}_c^{(g)}, \tag{19}$$

where the (g) superscript indicates a global matrix constructed from the modifiable sections and the previously coupled fixed sections.

Since, in this case, the interaction between the cylindrical ports of the fixed sections has already been performed, (7) is used to define a new coupling matrix

$$\mathbf{G}_c^{(g)} = \begin{pmatrix} \mathbf{G}_c^{mm} & \mathbf{G}_c^{mf} \\ \mathbf{G}_c^{fm} & \mathbf{0} \end{pmatrix}.$$

Similarly, the cylindrical scattering matrix, $\mathbf{S}_c^{(g)}$, should also consider independently the previously coupled fixed cylindrical modes to those corresponding to the modifiable sections, resulting in

$$\mathbf{S}_c^{(g)} = \begin{pmatrix} \mathbf{S}_c^m & \mathbf{0} \\ \mathbf{0} & \mathbf{S}_c^{(c)f} \end{pmatrix},$$

and since the feeding ports are contained in the fixed sections

$$\mathbf{T}_c^{(g)} = \begin{pmatrix} \mathbf{0} \\ \mathbf{T}_c^{(c)f} \end{pmatrix}, \tag{20}$$

$$\mathbf{R}_c^{(g)} = \begin{pmatrix} \mathbf{0} & \mathbf{R}_c^{(c)f} \end{pmatrix}, \tag{21}$$

$$\mathbf{\Gamma}^{(g)} = \left(\mathbf{\Gamma}^{(c)f} \right). \tag{22}$$

Additionally, because the radiating elements are considered only modifiable sections

$$\mathbf{C}_{ce}^{(g)} = \begin{pmatrix} \mathbf{C}_{ce}^{m} \\ \mathbf{0} \end{pmatrix},$$
$$\mathbf{C}_{ec}^{(g)} = \begin{pmatrix} \mathbf{C}_{ec}^{m} & \mathbf{0} \end{pmatrix}.$$

The main computational effort of evaluating (16) resides in the needed inversion of (17). We will use block-wise matrix inversion instead of a direct inverse, since the matrix to invert can be decomposed as

$$\mathbf{I} - \mathbf{S}_c^{(g)}\mathbf{G}_c^{(g)} = \begin{pmatrix} \mathbf{I} - \mathbf{S}_c^{m}\mathbf{G}_c^{mm} & -\mathbf{S}_c^{m}\mathbf{G}_c^{mf} \\ -\mathbf{S}_c^{m}\mathbf{G}_c^{fm} & \mathbf{I} \end{pmatrix}. \tag{23}$$

Consequently,

$$\begin{pmatrix} \mathbf{I} - \mathbf{S}_c^{m}\mathbf{G}_c^{mm} & -\mathbf{S}_c^{m}\mathbf{G}_c^{mf} \\ -\mathbf{S}_c^{(c)f}\mathbf{G}_c^{fm} & \mathbf{I} \end{pmatrix}^{-1} = \begin{pmatrix} \mathbf{V} & \mathbf{V}\mathbf{S}_c^{m}\mathbf{G}_c^{mf} \\ \mathbf{S}_c^{(c)f}\mathbf{G}_c^{fm}\mathbf{V} & \mathbf{I} + \mathbf{S}_c^{(c)f}\mathbf{G}_c^{fm}\mathbf{V}\mathbf{S}_c^{m}\mathbf{G}_c^{mf} \end{pmatrix}, \tag{24}$$

with

$$\mathbf{V} = \left(\mathbf{I} - \mathbf{S}_c^{m} \left(\mathbf{G}_c^{mm} + \mathbf{G}_c^{mf}\mathbf{S}_c^{(c)f}\mathbf{G}_c^{fm} \right) \right)^{-1}. \tag{25}$$

The inversion expressed in (24) is more efficient than a direct inversion, since it benefits from the fact that the inverse of an identity matrix is itself.

Now, defining

$$\mathbf{A} = \mathbf{G}_c^{mf}\mathbf{S}_c^{(c)f}\mathbf{G}_c^{fm},$$
$$\mathbf{B} = \mathbf{C}_{ec}^{m}\left(\mathbf{G}_c^{mm} + \mathbf{A}\right)\mathbf{V},$$

and inserting them into (18) and (19) gives

$$\mathbf{M} = \mathbf{I} - (\mathbf{S}_e + \mathbf{B}\mathbf{C}_{ce}^{m})\mathbf{G}_e, \tag{26}$$

$$\mathbf{Q} = \left(\mathbf{B}\mathbf{S}_c^{m} + \mathbf{C}_{ec}^{m}\right)\mathbf{G}_c^{mf}\mathbf{T}_c^{(c)f}. \tag{27}$$

The terms of (16) that included $\mathbf{P}$ are now expressed as

$$\mathbf{R}_c^{(g)}\mathbf{G}_c^{(g)}\mathbf{P}\mathbf{T}_c^{(g)} = \mathbf{R}_c^{(c)f}\mathbf{G}_c^{fm}\mathbf{V}\mathbf{S}_c^{m}\mathbf{G}_c^{mf}\mathbf{T}_c^{(c)f},$$
$$\mathbf{R}_c^{(g)}\mathbf{G}_c^{(g)}\mathbf{P}\mathbf{C}_{ce}^{(g)}\mathbf{G}_e = \mathbf{R}_c^{(c)f}\mathbf{G}_c^{fm}\mathbf{V}\mathbf{C}_{ce}^{m}\mathbf{G}_e.$$

Therefore, using (26) and (27), (16) is computed as

$$\Big[\mathbf{\Gamma}^{(c)f} + \mathbf{R}_c^{(c)f}\mathbf{G}_c^{fm}\mathbf{V}\left(\mathbf{S}_c^{m} + \mathbf{C}_{ce}^{m}\mathbf{G}_e\mathbf{M}^{-1}\mathbf{Q}\right)\mathbf{G}_c^{mf}\mathbf{T}_c^{(c)f}\Big]\,\mathbf{v} = \mathbf{w}. \tag{28}$$

When the number of fixed sections is much greater than the number of modifiable ones, an usual occurrence, the main computational cost is due to finding $\mathbf{A}$, which is obtained from the multiplication of 3 matrices. These have a dimension of $nm \times nf$, $nf \times nf$ and $nf \times nm$, where nf is the total number of cylindrical modes used in the considered fixed sections. nm, by contrast, is its counterpart for the considered modifiable sections. Nevertheless, the direct computation of (16), as it was done in [29], requires the inversion of a square matrix with dimension $(nm + nf) \times (nm + nf)$ to obtain $\mathbf{P}$ in each iteration. On the other hand, the effort to calculate $\mathbf{M}^{-1}\mathbf{Q}$ is identical to solving an equation system with a dimension equal to the number of spherical modes. For antennas placed on top of a SIW plate, the total number of used spherical modes is much lower than the number of used cylindrical modes, implying a much lower effort. The new strategy allows for faster iteration times in an optimization process, as it will be seen in the next section.

Regarding the radiated field, it can be obtained from the scattered vector spherical waves when the interactions between all the sections are taken into account [29]

$$\boldsymbol{E}\left(\hat{u}\right) = \mathbf{U}\mathbf{b}_e = \mathbf{U}\mathbf{F}\mathbf{M}^{-1}\mathbf{Q}\mathbf{v}, \tag{29}$$

where $\mathbf{F}$ accounts for the rotation angles if there are rotated elements [40]. $\mathbf{U}$ is

$$\mathbf{U} = \left(\boldsymbol{e}e^{-jk_0\hat{u}\cdot\boldsymbol{u}_1}, \ldots, \boldsymbol{e}e^{-jk_0\hat{u}\cdot\boldsymbol{u}_i}, \ldots, \boldsymbol{e}e^{-jk_0\hat{u}\cdot\boldsymbol{u}_{N_e}}\right), \tag{30}$$

where $\boldsymbol{u_i}$ is the position vector of the array element i, ($\boldsymbol{u_i} = x_i\hat{x} + y_i\hat{y}$), k_0 is the free space wavenumber, $\hat{u}$ is the unitary vector in spherical coordinates, and $\boldsymbol{e}$ is a row vector containing the electric fields of the spherical modes in each array element. From the calculated radiated field, any desired radiation pattern for a specified polarization can be easily computed.

III. Optimization process

In this section, a progressive-wave 16 transversal slot SIW-fed 1D linear array antenna polarized in x-direction, according to Fig. 3, is designed using the freely available unified third version of the non-dominated sorting genetic algorithm (U-NSGA-III) [41] provided with pymoo [42], considering Riesz s-Energy directions [43]. The NSGA-III gave excellent performance when used with a different strategy to optimize a slotted hollow rectangular waveguide in [**?**]. According to their authors, the U-NSGA-III algorithm, as well as the Riesz s-Energy directions, provide better convergence in multi-objective optimizations when compared to the original NSGA-III and Das-Dennis directions. They also ensure that a global optimized minimum can be reached in a many variables to optimize scenario. Nevertheless, any optimization algorithm can be seamlessly integrated to the proposed strategy.

The device is based on a Rogers RT/Duroid 5880 ($\varepsilon_r = 2.2$) substrate, with a height of $1.575\,\mathrm{mm}$ and a $35\,\mu\mathrm{m}$ copper thickness. The SIW width (w_{siw}) is $11\,\mathrm{mm}$, the via diameter (d) and pitch (p) are $0.8\,\mathrm{mm}$ and $1.6\,\mathrm{mm}$ respectively. Since an equivalent rectangular waveguide (RW) with the same

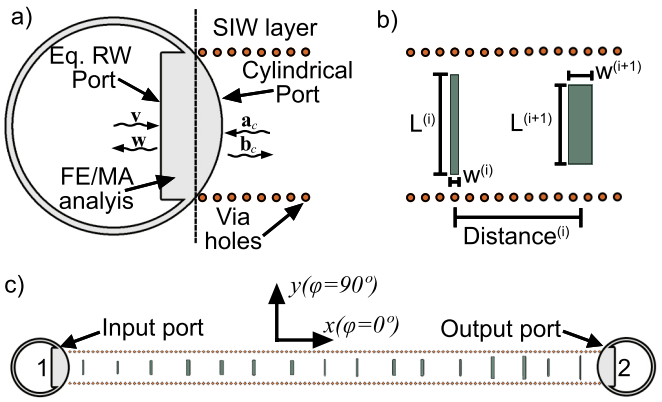

Figure 3. a) Top view of the equivalent RW to cylindrical port transition with connection to the SIW layer. b) Top view of two slots with their variables to optimize: length, width and distance between consecutive slots. c) Top schematic view of the optimized array with considered local axis.

propagation constant (β) can be determined, it is used as the excitation of the fundamental mode of the SIW in the array design process. The RW width is obtained using the equations from [44], resulting in a value of $10.573\,\mathrm{mm}$. A RW to cylindrical port transition is designed following the structure shown in Fig. 3.a, so that a back-to-back configuration with a SIW in between ensures a reflection coefficient under $-50\,\mathrm{dB}$. Two of these structures are used as the input and output ports of the device in the optimization process. The selected working frequency is $17\,\mathrm{GHz}$, suitable for satellite communications or radar positioning applications.

The parameters to optimize are the length and width of each individual slot, and the distance between consecutive slots, adding to a total of 47 individual variables to optimize. Broadside radiation in slot arrays usually implies matching problems due to the in-phase additive mismatches of each individual radiating element [45], [46], usually placed at the ideal distance of near a guided wavelength (λ_g) in hollow rectangular waveguides. Furthermore, the distance used to separate the slots results in grating lobes, greatly reducing the array performance. Since SIW is substrate based, the grating lobe problem is partially solved. However, the λ_g spacing needed for broadside radiation still implies the appearance of in-phase additive mismatches. Examples in the literature without additional matching elements, nor modifications to the radiating element, are hard to find [47], [4], [5], [7], [48], [12], [22]. Transversal arrays increment the matching problem not only due to their higher slot reflection, but also due to the effects of mutual coupling between individual slots [49], resulting in additional modifications to the design elements [21], [32], [20], [33], [34]. Additionally, they also usually employ a monotonically increasing slot length to obtain a near-broadside radiation, and use the slot width as a fixed parameter of the design. In this work, all these traditional problems are attempted to be solved with the selected optimized variables, which clearly go in contrast with previous works.

Four different optimization goals are defined as minimization functions. In terms of $|S_{11}|$, the goal is defined as a maximum difference between the obtained values and $-20\,\mathrm{dB}$ at $17\,\mathrm{GHz}$, and $-15\,\mathrm{dB}$ at $16.85\,\mathrm{GHz}$ and $17.15\,\mathrm{GHz}$. The purpose of this goal is to obtain a sufficiently wide bandwidth where the $|S_{11}|$ is under $-10\,\mathrm{dB}$. A lower than $-30\,\mathrm{dB}$ at $17\,\mathrm{GHz}$ goal is defined in the case of $|S_{21}|$. This $|S_{21}|$ goal will ensure that the incoming power is radiated through the slots, and will not escape through the output port. In the case of the gain in the array ($\varphi = 0°$) plane, the goal is defined as a minimization of the inverse of the maximum gain between $\theta = -10°$ and $\theta = 10°$ at $17\,\mathrm{GHz}$, in order to obtain maximum near-broadside radiation. The last goal is to minimize the side lobe level (SLL) in the same $\varphi = 0°$ plane at $17\,\mathrm{GHz}$. Transversal linear slot arrays have a very strong linearly polarized radiation pattern in the main direction of the array. Due to this, only goals on the array plane are considered for this optimization. Nevertheless, since the proposed strategy is able to fully determine the radiated field, optimization goals can be defined for any polarization or direction in accordance with the radiating element or the geometry.

The genetic algorithm is set up with a population size of 2350 individuals, a mutation η of 3, and a 100% probability of a binary crossover [50] with also an η of 3. As termination criteria, up to 48 generations will be calculated.

The distance between consecutive slots is optimized between $7.83\,\mathrm{mm}$ and $16.53\,\mathrm{mm}$ ($0.45\lambda_0$ and $0.95\lambda_0$, or $0.55\lambda_g$ and $1.15\lambda_g$ at $17\,\mathrm{GHz}$, respectively). The selected separations between slots, in a transversal array, make in-phase mismatching and mutual coupling effects possible to occur. Nevertheless, the proposed methodology can take them into account, ensuring that the optimized design has solved these problems. The length of the slots is discretized into 32 values, ranging from $4.0\,\mathrm{mm}$ to $8.65\,\mathrm{mm}$ ($0.23\lambda_0$ and $0.50\lambda_0$, respectively). The width, on the other hand, varies from $0.3\,\mathrm{mm}$ to $1.2\,\mathrm{mm}$, and is discretized into 7 values. A FE/MA of each possible section is carried out to obtain their corresponding GSMs, using 24 spherical and 15 cylindrical modes in their respective spherical and cylindrical ports. The SIW vias are described analytically using 7 cylindrical modes, while 21 cylindrical modes are used for the RW feeding section.

To guarantee that all the possible combinations of parameters can be simulated, the 16 slots are placed along a $259.2\,\mathrm{mm}$ ($14.5\lambda_0$) long SIW. With this, the 16 antennas can be separated by the maximum possible distance, and still have a $5\,\mathrm{mm}$ separation from the feeders. Therefore, the considered fixed sections are the two RW to cylindrical port transitions, and 162 pairs of metallized via holes, resulting in 2310 fixed cylindrical modes. The modifiable sections, which are the antennas, account for a total of 384 spherical modes and 240 cylindrical modes.

Table I shows a comparison of the CPU execution time per calculated frequency point between using the FEM solver from CST Studio Suite 2020, the previous work published in [29] and this work. This comparison is subdivided in GSMs computation (using the FE/MA solver), analysis time and iteration time. The GSMs computation time is the time spent by the FE/MA solver to obtain the GSM of the equivalent RW feeder and each one of the 224 possible slot combinations (32 lengths with 7 widths). It must be noted that the GSM are only computed once, at the start of the optimization process.

Table I
CPU SIMULATION TIME PER CALCULATED FREQUENCY POINT ON A XEON E-2176G (3.70 GHz) FOR THE PERFORMED OPTIMIZATION PROCESS.

	CST	Using [29]	This work
GSM computation (Step 0)	N.A.	805.1 s	805.1 s
Analysis time (Steps 1+2)	282.36 s	1.21 s	1.53 s
Iteration time (Step 2)	282.36 s	1.21 s	0.12 s
Iteration speedup factor (compared to CST)	x1	x233	x2259

Analysis time refers to the time needed to obtain the complete response of the device from the start of the optimization process. For the new proposed strategy, this means the time spent in firstly calculating the interaction of the fixed sections, and then coupling the modifiable section. Iteration time refers to the time needed to obtain the complete response of the device when some part of it is modified. While for the previous work in [29], and with many commercial software, this implies to restart the whole calculation process, for the new strategy it implies that only the coupling to modifiable section has to be redone. This key difference allows for speedup factors of over x2000 for the performed optimization process when compared to commercial software.

This speedup factor implies that if single frequency optimization goals are defined, the complete optimization process (112800 total iterations), with full-wave accuracy in the result obtained in each iteration, takes 4 hours to finish with the new proposed strategy. In contrast, the same optimization process using the findings in [29] would take 38 hours to complete, while the use of the general purpose CST Studio Suite would be unaffordable, leaving its use for the subsequent validation step.

IV. VALIDATION AND RESULTS

This section features a comparison between the results obtained from the proposed full-wave methodology, CST Studio Suite 2020 and experimental measurements. The optimized physical dimensions of each slot, as also the separation between them, are shown in Table II. The distance between slots is defined from one slot to the next. In other words, the separation indicated for the first slot represents the distance between the centers of the first and the second slot.

The optimized design is also simulated with CST Studio Suite 2020, in order to validate the full-wave capabilities of the proposed methodology. The obtained results are shown in Fig. 4, where an excellent agreement between the two software can be observed. In terms of $|S_{11}|$, not only are the defined optimization goals completely fulfilled, but a $1.05\,\mathrm{GHz}$ bandwidth under $-10\,\mathrm{dB}$, from $16.32\,\mathrm{GHz}$ to $17.37\,\mathrm{GHz}$, is also obtained. The $|S_{21}|$ of these two lossless simulations has a $-50\,\mathrm{dB}$ value at $17\,\mathrm{GHz}$, so it can be considered negligible.

Regarding the simulated gain at $17\,\mathrm{GHz}$, a maximum value of $17.5\,\mathrm{dBi}$ at $\theta = -10^\circ$ in the array ($\varphi = 0^\circ$) plane is obtained. The maximum obtained gain for the cross-polarization

Table II
OPTIMIZED DIMENSIONS AND SEPARATION OF THE 16 SLOTS.

Slot Number	Length (mm)	Width (mm)	Distance (mm)
1	4.60	0.60	12.00
2	4.75	0.75	11.14
3	5.20	1.05	12.23
4	5.35	0.45	10.86
5	5.50	1.20	11.55
6	5.65	1.05	10.18
7	5.20	1.20	13.01
8	5.50	1.20	10.27
9	5.65	1.05	10.30
10	6.55	0.30	9.45
11	6.40	1.20	9.28
12	6.70	0.90	11.81
13	6.25	0.30	9.26
14	7.15	0.45	8.54
15	7.15	0.75	9.62
16	7.30	0.30	-

is $-46.4\,\mathrm{dBi}$ with the proposed strategy, and $-59.8\,\mathrm{dBi}$ with CST Studio Suite. The total efficiency of an array is defined as the realized gain divided by its directivity. In these lossless simulations, the total efficiency of the design is equal to the ratio of the power accepted by the antenna to the power incident at the antenna terminals. This parameter, also called impedance mismatch factor (M), is calculated for this 2-port antenna as $1-|S_{11}|^2-|S_{21}|^2$, resulting in a total 99.95% efficiency. When the datasheet dielectric and metal losses are considered, the maximum realized gain value descends to $17\,\mathrm{dBi}$. The total efficiency in this case can also be expressed as M/l, where l refers to the the considered losses in natural units, calculated as $l = 10^{\frac{L(\mathrm{dB})}{10}}$ (with $L(\mathrm{dB})$ being the positive losses in dB of the device). For the considered datasheet dielectric and metal losses, the simulated total efficiency is reduced to 88.0% The obtained SLL is $-13.6\,\mathrm{dB}$, while the angular width at $3\,\mathrm{dB}$ is 7°. When losses are considered, the maximum obtained gain for the cross-polarization is $-65.0\,\mathrm{dBi}$, according to CST Studio Suite.

The design is manufactured and measured, and its radiation pattern is characterized. A $2.2\,\mathrm{mm}$ wide and $8.0\,\mathrm{mm}$ long microstrip line, as seen in [7], is added to the device to match a Huber+Suhner end-launch SMA connector. The manufactured design has a total length of $22.08\,\mathrm{cm}$, while the distance between the first and last slot is $15.95\,\mathrm{cm}$, which equates to $9.17\lambda_0$ at $17\,\mathrm{GHz}$. An additional SIW with the same length as the antenna is also produced to correctly characterize the chosen substrate. Photos of the manufactured device, as also various photos of the measurement process, are exhibited in Fig. 5.

In order to consider the real effects on transmission due to substrate tolerances, and losses due to connectors and the chosen coaxial to SIW transition, the manufactured SIW with the same length as the antenna is experimentally characterized. The obtained results are used to model the unforeseen realistic effects. The substrate is now modeled with a dielectric constant of $\varepsilon_r = 2.18$, and an experimentally adjusted tangent loss of 0.004 that covers all the mentioned realistic effects. An additional simulation, considering the used connectors, the coaxial

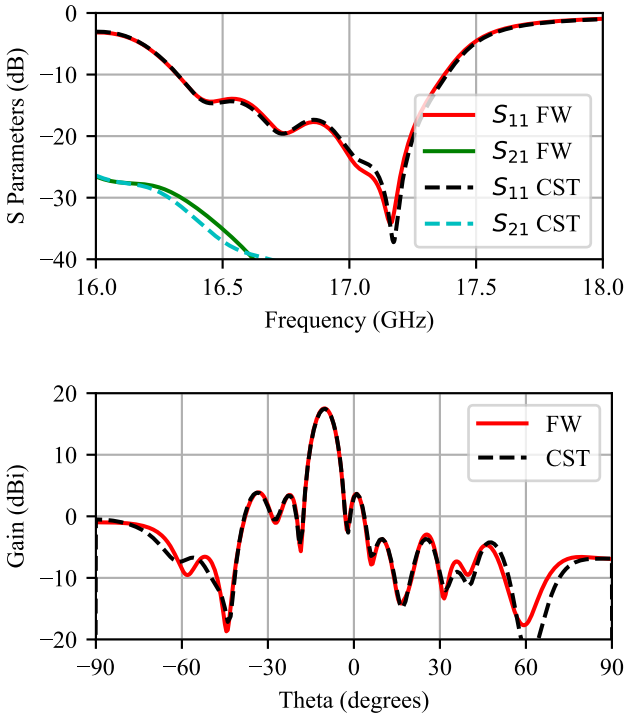

Figure 4. Simulated s-parameters (top) and realized gain at 17 GHz in the $\varphi = 0°$ plane (bottom) of the lossless optimized design. FW refers to the results obtained with the proposed full-wave methodology.

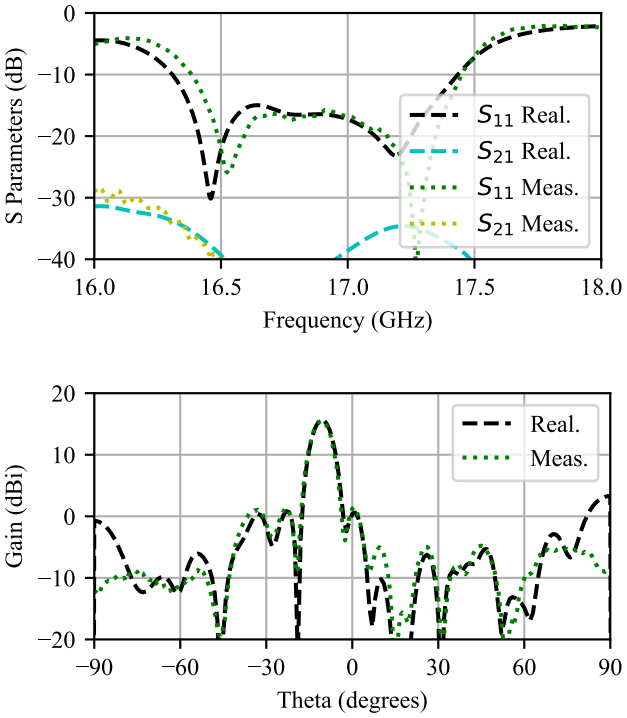

Figure 6. S-parameters (top) and realized gain at 17 GHz in the $\varphi = 0°$ plane (bottom) measured (Meas.) and simulated with CST Studio Suite 2020 in realistic conditions (Real.).

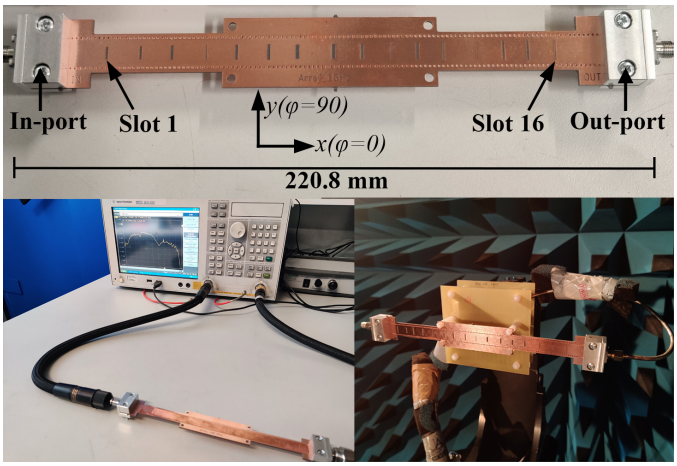

Figure 5. Photo of: manufactured optimized design with end-launch connectors (top), substrate characterization using a SIW of the same length (left), and radiation measurement mount in an anechoic chamber (right).

to SIW transition, the effects due to the rounded corners of the slots because of fabrication limits, the measured substrate characterization data, and the copper surface roughness, is performed.

The results obtained from the measurement process, as also from the simulation in realistic conditions, are shown in Fig. 6. These exhibit a close resemblance in terms of s-parameters, albeit with a slight frequency shift. The measurements show a $|S_{11}|$ $-10\,\mathrm{dB}$ band of $1.06\,\mathrm{GHz}$, from $16.38\,\mathrm{GHz}$ to $17.44\,\mathrm{GHz}$. In the case of the simulation, this bandwidth is expanded to $1.13\,\mathrm{GHz}$, from $16.30\,\mathrm{GHz}$ to $17.43\,\mathrm{GHz}$. At $17\,\mathrm{GHz}$, the measured $|S_{21}|$ is $-50\,\mathrm{dB}$. And while the SLL and the angular width have been maintained, the maximum realized gain has been reduced to $15.6\,\mathrm{dBi}$. Also, because of the dielectric constant variation and the rounded slot corners, the maximum gain is now located at $\theta = -11°$ in the $\varphi = 0°$ plane. The increased losses imply that a total efficiency of 64.5% is obtained from the measurements, while a M of 98.5% is measured. Although CST Studio Suite predicts a maximum cross-polarization gain of $-63.0\,\mathrm{dBi}$, the measured value was $-22.3\,\mathrm{dBi}$.

Fig. 7 shows the maximum realized gain and total efficiency, over frequency, measured and simulated with CST Studio Suite 2020 with datasheet values and realistic conditions. A great resemblance between the obtained results can be observed not only for the design frequency, but also over most of the obtained bandwidth in which $|S_{11}|$ is under $-10\,\mathrm{dB}$. The measured $3\,\mathrm{dBi}$ gain bandwidth is $1.33\,\mathrm{GHz}$, from $16.23\,\mathrm{GHz}$ to $17.56\,\mathrm{GHz}$. In terms of total efficiency, a minimum value of 60% measured between $16.45\,\mathrm{GHz}$ and $17.46\,\mathrm{GHz}$, although a 95% of matched power is measured between $16.42\,\mathrm{GHz}$ and $17.42\,\mathrm{GHz}$

Although the measurements show a decreased performance with respect to the original simulations of the optimized device, all the goals proposed in the optimization process have been correctly fulfilled. Furthermore, the measurements show how the obtained design is robust to fabrication errors and substrate realistic effects. The main drawback observed in the measurements is attributed to greater than expected losses,

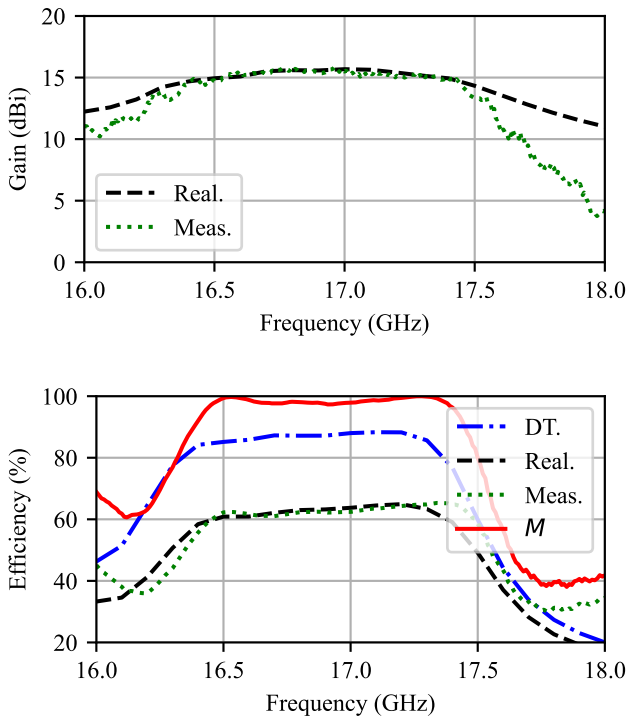

Figure 7. Maximum realized gain over frequency (top) and total efficiency (bottom) measured (Meas.) and simulated with CST Studio Suite 2020 in datasheet (DT.) and realistic (Real.) conditions. Bottom graphic also shows the measured impedance mismatch factor (M).

which in this specific optimization process have not been taken into account.

V. Conclusion

In this work, we have introduced a new strategy that greatly reduces iteration times in an array design and optimization process. Its usefulness has been validated by performing a complete design process of a novel 16-slot progressive-wave SIW-fed array. The inclusion of the coupling between radiating elements in the optimization phase has resulted in a non-traditional design, with no monotonic tendencies and no additional matching elements being used. This has been, traditionally, a difficult task, because of the strong mutual coupling and matching problems due to the chosen polarization and near-broadside radiation. The optimization process has been carried out in 12 hours (4 hours per optimized frequency point), resulting in extreme speedup factors compared to traditional commercial software. Furthermore, the full-wave capabilities of the methodology have been validated by CST Studio Suite 2020. The designed array has been manufactured and experimentally characterized, resulting in a great resemblance to simulations with realistic conditions. Therefore, the new strategy allows quick design processes, even with a high number of optimization variables, and providing full-wave accuracy in the results of each iteration.

Acknowledgment

The authors would like to thank Pablo Sánchez-Olivares, from the Polytechnic University of Madrid, for facilitating the access to his previous work published in [7].

References

[1] D. Deslandes and K. Wu, "Integrated microstrip and rectangular waveguide in planar form," *IEEE Microw. Wireless Compon. Lett.*, vol. 11, no. 2, pp. 68–70, 2001.

[2] K. Wu, D. Deslandes, and Y. Cassivi, "The substrate integrated circuits-A new concept for high-frequency electronics and optoelectronics," in *Proc. 6th Int. Conf. Telecommun. Modern Satellite Cable and Broadcasting*, vol. 1, 2003, pp. P–III–P–X.

[3] L. Yan, W. Hong, G. Hua, J. Chen, K. Wu, and T. J. Cui, "Simulation and experiment on SIW slot array antennas," *IEEE Microw. Wireless Compon. Lett.*, vol. 14, no. 9, pp. 446–448, 2004.

[4] P. Chen, W. Hong, Z. Kuai, and J. Xu, "A substrate integrated waveguide circular polarized slot radiator and its linear array," *IEEE Antennas Wireless Propag. Lett.*, vol. 8, pp. 120–123, 2009.

[5] J. L. Masa-Campos, P. Rodríguez-Fernández, M. Sierra-Pérez, and J. L. Fernández-Jambrina, "Monopulse circularly polarized SIW slot array antenna in millimetre band," *J. Electromagn. Waves Appl.*, vol. 25, no. 5-6, pp. 857–868, 2011.

[6] S. E. Hosseininejad and N. Komjani, "Optimum design of traveling-wave SIW slot array antennas," *IEEE Trans. Antennas Propag.*, vol. 61, no. 4, pp. 1971–1975, 2013.

[7] P. Sanchez-Olivares and J. L. Masa-Campos, "Novel four cross slot radiator with tuning vias for circularly polarized SIW linear array," *IEEE Trans. Antennas Propag.*, vol. 62, no. 4, pp. 2271–2275, 2014.

[8] Y. F. Wu and Y. J. Cheng, "Conical conformal shaped-beam substrate-integrated waveguide slot array antenna with conical-to-cylindrical transition," *IEEE Trans. Antennas Propag.*, vol. 65, no. 8, pp. 4048–4056, 2017.

[9] A. Dewantari, J. Kim, I. Scherbatko, and M. H. Ka, "A sidelobe level reduction method for mm-wave substrate integrated waveguide slot array antenna," *IEEE Antennas Wireless Propag. Lett.*, vol. 18, no. 8, pp. 1557–1561, 2019.

[10] J. Xiao, Z. Qi, X. Li, and H. Zhu, "Broadband and high-gain SIW-fed slot array for millimeter-wave applications," *IEEE Trans. Antennas Propag.*, vol. 67, no. 5, pp. 3484–3489, 2019.

[11] H. Bai, G. ming Wang, X. jun Zou, and T. Wu, "Wideband and gain enhancement SIW slot array antenna using sparsification processing and composite metasurface," *IEEE Trans. Antennas Propag.*, vol. 69, no. 12, pp. 9009–9014, 2021.

[12] A. A. Diman, F. Karami, P. Rezaei, A. Amn-E-Elahi, Z. Mousavirazi, T. A. Denidni, and A. A. Kishk, "Efficient SIW-feed network suppressing mutual coupling of slot antenna array," *IEEE Trans. Antennas Propag.*, vol. 69, no. 9, pp. 6058–6063, 2021.

[13] W. M. Abdel-Wahab, Y. Wang, and S. Safavi-Naeini, "SIW hybrid feeding network-integrated 2-D DRA array: Simulations and experiments," *IEEE Antennas Wireless Propag. Lett.*, vol. 15, pp. 548–551, 2016.

[14] M. S. Abdallah, Y. Wang, W. M. Abdel-Wahab, and S. Safavi-Naeini, "Design and optimization of SIW center-fed series rectangular dielectric resonator antenna array with 45° linear polarization," *IEEE Trans. Antennas Propag.*, vol. 66, no. 1, pp. 23–31, 2018.

[15] N. K. Mallat and A. Iqbal, "Out-of-band suppressed SIW-DRA based filter-antenna subsystem with flexible bandwidth and transmission zeros," *AEU - Int. J. Electron. Commun.*, vol. 135, p. 153735, 2021.

[16] D. Y. Kim, J. W. Lee, T. K. Lee, and C. S. Cho, "Design of SIW cavity-backed circular-polarized antennas using two different feeding transitions," *IEEE Trans. Antennas Propag.*, vol. 59, no. 4, pp. 1398–1403, 2011.

[17] Q. Yang, S. Gao, Q. Luo, L. Wen, Y. L. Ban, X. Ren, J. Wu, X. Yang, and Y. Liu, "Millimeter-wave dual-polarized differentially fed 2-D multibeam patch antenna array," *IEEE Trans. Antennas Propag.*, vol. 68, no. 10, pp. 7007–7016, 2020.

[18] H. Liu, A. Qing, Z. Xu, Z. Yu, and S. Zhang, "Design of physically connected wideband SIW cavity-backed patch antenna for wide-angle scanning phased arrays," *IEEE Antennas Wireless Propag. Lett.*, vol. 20, no. 3, pp. 406–410, 2021.

[19] Q. Yang, S. Gao, Q. Luo, L. Wen, Y. L. Ban, X. X. Yang, X. Ren, and J. Wu, "Cavity-backed slot-coupled patch antenna array with dual slant polarization for millimeter-wave base station applications," *IEEE Trans. Antennas Propag.*, vol. 69, no. 3, pp. 1404–1413, 2021.

[20] A. M. Malekshah, A. R. Attari, and M. S. Majedi, "Improved design of uniform SIW leaky wave antenna by considering the unwanted mode," *IEEE Trans. Antennas Propag.*, vol. 68, no. 8, pp. 6378–6382, 2020.
[21] D. Zheng, Y. L. Lyu, and K. Wu, "Transversely slotted SIW leaky-wave antenna featuring rapid beam-scanning for millimeter-wave applications," *IEEE Trans. Antennas Propag.*, vol. 68, no. 6, pp. 4172–4185, 2020.
[22] M. Z. Ali and Q. U. Khan, "High gain backward scanning substrate integrated waveguide leaky wave antenna," *IEEE Trans. Antennas Propag.*, vol. 69, no. 1, pp. 562–565, 2021.
[23] L. Liu, T. L. Bai, J. Y. Deng, D. Sun, Y. Zhang, T. Yong, S. G. Zhou, and L. X. Guo, "Substrate integrated waveguide filtering horn antenna facilitated by embedded via-hole arrays," *IEEE Antennas Wireless Propag. Lett.*, vol. 19, no. 7, pp. 1187–1191, 2020.
[24] Y. Zhang, J. Y. Deng, D. Sun, J. Y. Yin, and L. X. Guo, "Compact slow-wave SIW H-plane horn antenna with increased gain for vehicular millimeter wave communication," *IEEE Trans. Veh. Technol.*, vol. 70, no. 7, pp. 7289–7293, 2021.
[25] Y. Yu, W. Hong, H. Zhang, J. Xu, and Z. H. Jiang, "Optimization and implementation of SIW slot array for both medium- and long-range 77 GHz automotive radar application," *IEEE Trans. Antennas Propag.*, vol. 66, no. 7, pp. 3769–3774, 2018.
[26] M. Casaletti, G. Valerio, J. Seljan, M. Ettorre, and R. Sauleau, "A full-wave hybrid method for the analysis of multilayered SIW-based antennas," *IEEE Trans. Antennas Propag.*, vol. 61, no. 11, pp. 5575–5588, 2013.
[27] M. Bertrand, G. Valerio, M. Ettorre, and M. Casaletti, "RWG basis functions for accurate modeling of substrate integrated waveguide slot-based antennas," *IEEE Trans. Magn.*, vol. 56, no. 1, pp. 1–4, 2020.
[28] J. Rubio, A. G. García, R. G. Alcalá, Y. Campos-Roca, and J. Zapata, "Overall formulation for multilayer SIW circuits based on addition theorems and the generalized scattering matrix," *IEEE Microw. Wireless Compon. Lett.*, vol. 28, no. 6, pp. 485–487, 2018.
[29] J. Rubio, A. G. García, R. G. Alcalá, J. García, and Y. Campos-Roca, "Simultaneous use of addition theorems for cylindrical and spherical waves for the fast full-wave analysis of SIW-based antenna arrays," *IEEE Trans. Antennas Propag.*, vol. 67, no. 12, pp. 7379–7386, 2019.
[30] J. Corcoles, P. Sanchez-Olivares, J. Rubio, J. L. Masa-Campos, and J. Zapata, "Computer automated design of an irregular slotted waveguide array for Ku-Band," *IEEE Antennas Wireless Propag. Lett.*, vol. 15, pp. 1593–1597, 2016.
[31] C. S. Technology and Dassault Systèmes Vélizy-Villacoublay France, "Cst Studio Suite ™ 2020," https://www.cst.com/, 2010. [Online]. Available: https://www.3ds.com/es/productos-y-servicios/simulia/productos/cst-studio-suite/
[32] D. Zheng and K. Wu, "Multifunctional filtering leaky-wave antenna exhibiting simultaneous rapid beam-scanning and frequency-selective characteristics based on radiative bandpass filter concept," *IEEE Trans. Antennas Propag.*, vol. 68, no. 8, pp. 5842–5854, 2020.
[33] N. Javanbakht, B. Syrett, R. E. Amaya, and J. Shaker, "A Review of reconfigurable leaky-wave antennas," vol. 9, pp. 94 224–94 238, 2021.
[34] D. K. Karmokar, D. N. Thalakotuna, L. Matekovits, and K. P. Esselle, "One dimensional leaky-wave antennas with continuous scan of radiating beam," in *2021 International Conference on Electromagnetics in Advanced Applications, ICEAA 2021*. Institute of Electrical and Electronics Engineers Inc., 2021, pp. 101–103.
[35] A. D. Yaghjian, *Near-field antenna measurements on a cylindrical surface: A source-scattering matrix formulation*. Boulder, Colorado: Department of Commerce, National Bureau of Standards, Institute for Basic Standards, Electromagnetics Division., 1977, vol. 696. [Online]. Available: https://nvlpubs.nist.gov/nistpubs/Legacy/TN/nbstechnicalnote696.pdf
[36] J. E. Hansen, *Spherical near-field antenna measurements*. London, UK: Peter Peregrinus Ltd., 1988, vol. 26.
[37] E. Díaz Caballero, H. Esteban, Á. Belenguer, and V. Boria, "Efficient analysis of substrate integrated waveguide devices using hybrid mode matching between cylindrical and guided modes," *IEEE Trans. Microw. Theory Tech.*, vol. 60, no. 2, pp. 232–243, 2012.
[38] J. Rubio, M. A. González, and J. Zapata, "Generalized-scattering-matrix analysis of a class of finite arrays of coupled antennas by using 3-D FEM and spherical mode expansion," *IEEE Trans. Antennas Propag.*, vol. 53, no. 3, pp. 1133–1144, 2005.
[39] J. F. Izquierdo, J. Rubio, and J. Zapata, "Antenna-generalized scattering matrix in terms of equivalent infinitesimal dipoles: Application to finite array problems," *IEEE Trans. Antennas Propag.*, vol. 60, no. 10, pp. 4601–4609, 2012.
[40] J. I. Echeveste, J. Rubio, M. Á. De Aza, and C. Craeye, "Pattern synthesis of coupled antenna arrays via element rotation," *IEEE Antennas Wireless Propag. Lett.*, vol. 16, pp. 1707–1710, 2017.
[41] H. Seada and K. Deb, "A unified evolutionary optimization procedure for single, multiple, and many objectives," *IEEE Trans. Evol. Comput.*, vol. 20, no. 3, pp. 358–359, 2016.
[42] J. Blank and K. Deb, "Pymoo: Multi-objective optimization in Python," vol. 8, pp. 89 497–89 509, 2020.
[43] J. Blank, K. Deb, Y. Dhebar, S. Bandaru, and H. Seada, "Generating well-spaced points on a unit simplex for evolutionary many-objective optimization," *IEEE Trans. Evol. Comput.*, vol. 25, no. 1, pp. 48–60, 2021.
[44] F. Xu and K. Wu, "Guided-wave and leakage characteristics of substrate integrated waveguide," *IEEE Trans. Microw. Theory Tech.*, vol. 53, no. 1, pp. 66–72, 2005.
[45] J. L. Masa-Campos, J. M. Fernández, M. Sierra-Pérez, and J. L. Fernández-Jambrina, "Omnidirectional circularly polarized slot antenna fed by a cylindrical waveguide in millimeter band," *Microw. Opt. Technol. Lett.*, vol. 49, no. 3, pp. 638–642, 2007.
[46] H. Yi, L. Li, J. Han, and Y. Shi, "Traveling-wave series-fed patch array antenna using novel reflection-canceling elements for flexible beam," vol. 7, pp. 111 466–111 476, 2019.
[47] Q. Zhang and Y. Lu, "45° Linearly polarized substrate integrated waveguide-fed slot array antennas," in *2008 International Conference on Microwave and Millimeter Wave Technology Proceedings, ICMMT*, vol. 3, 2008, pp. 1214–1217.
[48] R. Ranjan and J. Ghosh, "SIW-based leaky-wave antenna supporting wide range of beam scanning through broadside," *IEEE Antennas Wireless Propag. Lett.*, vol. 18, no. 4, pp. 606–610, 2019.
[49] T. Mikulasek, J. Puskely, A. G. Yarovoy, J. Lacik, and H. Arthaber, "Transverse slot with control of amplitude and phase for travelling-wave SIW antenna arrays," *IET Microw. Antennas Propag.*, vol. 14, no. 15, pp. 2007–2010, 2020.
[50] K. Deb, K. Sindhya, and T. Okabe, "Self-adaptive simulated binary crossover for real-parameter optimization," in *Proceedings of GECCO 2007: Genetic and Evolutionary Computation Conference*. New York, New York, USA: ACM Press, 2007, pp. 1187–1194.

Alfonso Gómez García was born in Córdoba, Andalusia, Spain in 1994. He received the B.S. and M.S. degrees with honors in telecommunications engineering from the University of Extremadura, Cáceres, in 2016 and 2018, respectively. He is currently pursuing the Ph.D. degree in electromagnetic engineering at University of Extremadura.

Since 2018, he is a Professor Assistant with the Departamento de Tecnología de Computadores y Comunicaciones, University of Extremadura. His research includes applications of a finite element/modal analysis method for microwave circuits and antennas, and the design and characterization of SIW based microwave antennas and circuits.

Jesús Rubio was born in Talavera de la Reina, Toledo, Spain, 1971. He received the M.S. and the Ph.D. degrees in telecommunication engineering from the Universidad Politécnica de Madrid, Spain, in 1995 and 1998, respectively.

Since 1994 he has collaborated with the Departamento de Electromagnetismo y Teoría de Circuitos of the Universidad Politécnica de Madrid. At present, he is working with the Departamento de Tecnología de Computadores y Comunicaciones of theUniversidad de Extremadura as a professor. His current research interests are in the application of the finite element method and modal analysis to passive microwave circuits problems and antennas.

Jose Luis Masa Campos was was born in Madrid, Spain, in 1974. He received the Master degree in 1999 and the Ph.D. Degree in 2006, from the Universidad Politécnica de Madrid, Spain.

From 1990 to 2003 we developed his professional activity in the R& D department of the company RYMSA with the design of base station antennas for mobile communications and satellite antennas. From 2002 to 2003 he directed the R& D department of RYMSA. From 2003 to 2007 he worked as Researcher for Universidad Politécnica de Madrid, and in 2005 he joined to Universidad Autónoma de Madrid as Associate Professor in the Radiofrequency Group (RFCAS).

His main current research interests are in active and passive planar array antennas (microstrip, substrate integrated waveguide or metallic waveguide technologies), associated antenna feeding networks and new additive manufacturing techniques applied to microwave circuits and antennas.

Juan Córcoles was born in Albacete, Spain, in 1981. He received the Ingeniero de Telecomunicación degree (the B.Sc. and M.Sc. degrees in electrical engineering) and the Doctor Ingeniero de Telecomunicación degree (the Ph.D. degree in electrical engineering) from the Universidad Politécnica de Madrid, Spain, in 2004 and 2009, respectively, the Diplomado en Ciencias Empresariales degree (the B.Sc. degree in business science) from the Universidad Complutense de Madrid, in 2008, and the Licenciado en Economía degree (the M.Sc. degree in Economics) from the Universidad Nacional de Educación a Distancia, Madrid, Spain, in 2010.

He was a Visiting Researcher with the Institut für Hochfrequenztechnik und Elektronik (IHE), Universität Karlsruhe (TH), Germany, from November 2008 to March 2009, IT'IS Foundation, ETHZ, Zurich, Switzerland, from July 2013 to September 2013 and June 2016 and August 2016, and King's College London, U.K., from October 2018 to December 2018. Since 2010, he has been with the Universidad Autónoma de Madrid, Spain, where he became an Associate Professor, in 2015.

His current research interests are in computational electromagnetics, particularly in the development and application of numerical methods and optimization techniques to the analysis and design of microwave circuits and antennas, especially antenna arrays, as well as to medical and other novel applications of radiofrequency electromagnetic fields.

Yolanda Campos Roca was born in Guitiriz (Lugo, Spain) in 1970. She received the M. S. and Ph.D. Degrees in Telecommunication Engineering from the Universidade de Vigo (Vigo, Spain), in 1994 and 2000, respectively. Her Ph.D. dissertation concerned the design of millimeter-wave frequency multipliers.

From 1996 to 2000, she performed research stays that accumulate almost three years at the Fraunhofer Institute for Applied Solid State Physics in Freiburg, Germany, either as a guest researcher from the University of Vigo or as a staff member. In 2000, she joined the University of Extremadura, Cáceres, Spain, as an Assistant Professor, becoming an Associate Professor in 2002. Her current research interests include circuit design in the microwave and millimeter-wave range and speech processing for biomedical applications.

Rafael Gómez Alcalá (M'01) was born in Córdoba, Spain in 1965. He received the degree in telecommunication engineering and the Ph.D. degree in telecommunication from the University of Vigo, Pontevedra, Spain, in 1990 and in 1996, respectively.

In 1999, he moved to the University of Extremadura, Cáceres, Spain, where he is currently a Faculty Member of the Polytechnic School of Cáceres. His research interests include microwave filters and antenna design.